Vortex chaoticons in thermal nonlocal nonlinear media

Qing Wang [1,2] Milivoj R. Belić,[3] Dumitru Mihalache [4] Liangwei Zeng,[5] Lingling Zhang,[2,*] and Ji Lin [1,†]

[1]*Department of Physics, Zhejiang Normal University, Jinhua 321004, China*
[2]*College of Science, JiuJiang University, Jiujiang 334000, China*
[3]*Texas A & M University at Qatar, Doha 23874, Qatar*
[4]*Horia Hulubei National Institute of Physics and Nuclear Engineering, Magurele, Bucharest, RO-077125, Romania*
[5]*College of Physics and Optoelectronic Engineering, Shenzhen University, Shenzhen 518060, China*

This paper numerically investigates the propagation of Laguerre-Gaussian vortex beams launched in nonlocal nonlinear media, such as lead glass. Our results show that the propagation properties depend on the selection of beam parameters m and p, which represent the azimuthal and radial mode numbers. When $p = 0$, these profiles can be stable solitons for $m \leqslant 2$, or break up and then form a set of single-hump profiles for $m \geqslant 3$, which are unbounded states with scattered remnants of the energy. However, for $p \geqslant 1$, the broken beams can evolve into vortex chaoticons, which exhibit both chaotic and solitonlike properties. The chaotic properties are determined by the positive Lyapunov exponents and spatial decoherence, while the solitonlike properties are demonstrated by the invariance of beam width and the interaction of beams in the form of quasielastic collisions. In addition, the power and orbital angular momentum of unbounded beam states both decay in propagation, while those of the chaoticons maintain their values well.

I. INTRODUCTION

Vortex beams display some unique characteristics, such as a helical wavefront, vanishing intensity at the center, and carrying orbital angular momentum (OAM), which make them of great applicative value in different fields of physics [1,2]. For example, the helical wavefront and spatial propagation invariance result in the vortex beams being used for free-space information transfer and communications [3,4]. Due to zero-central intensity, the vortex beam can form a potential well, to capture and manipulate particles [5,6]. Additionally, the OAM of a vortex beam can drive particles to rotate, which can be used as an optical wrench, optical tweezer, optical motor, and so on [7,8]. Owing to their application potential, researchers in different fields have used various methods to obtain vortex beams with different properties, including perfect vortex beams [9], vector vortex beams [10], broadband vortex beams [11], and terahertz vortex beams [12].

In a nonlinear medium, the soliton may form as a result of the self-focusing balancing the diffraction [13,14].In particular, the nonlocal nonlinearity exhibits interesting stabilizing characteristics, such as suppressing the collapse of (2+1)-dimensional optical beams [15], overcoming the instability of vortex beams [16], and others. As a consequence, a variety of solitons, such as Laguerre-Gaussian (LG) vortex solitons [17], imaginary value off-axis vortex solitons [18], spiraling elliptic solitons [19], spiraling anomalous vortex beam arrays [20],

and ring dark and antidark solitons [21], have been reported in nonlocal nonlinear media.

Furthermore, the stability of vortex solitons in different nonlocal nonlinear systems is different, and their stability is also related to the topological charge; for example, the maximum allowed m for a single-ring ($p = 0$) stable vortex soliton in actual nonlocal media has been revealed to be not more than 2 [22–24]. However, the evolution of higher-order LG beams has not been thoroughly discussed in actual nonlocal media, to the best of our knowledge. In fact, the study of higher-order LG beams, which are carrying more information, deserves more attention.

In addition, unlike the local nonlinear, the nonlocal nonlinear model as a rule is nonintegrable and cannot be solved analytically. In a nonintegrable nonlinear system, the higher-order beams often evolve into chaos, but recently it has been shown that some beams may evolve into chaoticons, unique chaotic states that also exhibit solitonlike properties [25]. Chaoticons, as a new kind of beam occurring in nonlocal nonlinear media, whose existence modes are different from the chaoticons in dissipative systems [26,27], have become an interesting research topic. In this sense, it is worth discussing (1) whether the evolution of higher-order vortex beams in nonlocal media can evolve into chaoticons or not, and (2) the variation of beam power and OAM. These issues are investigated in this paper.

II. THEORETICAL MODEL

The propagation of an optical beam in lead glass can be described by the two-dimensional dimensionless nonlocal
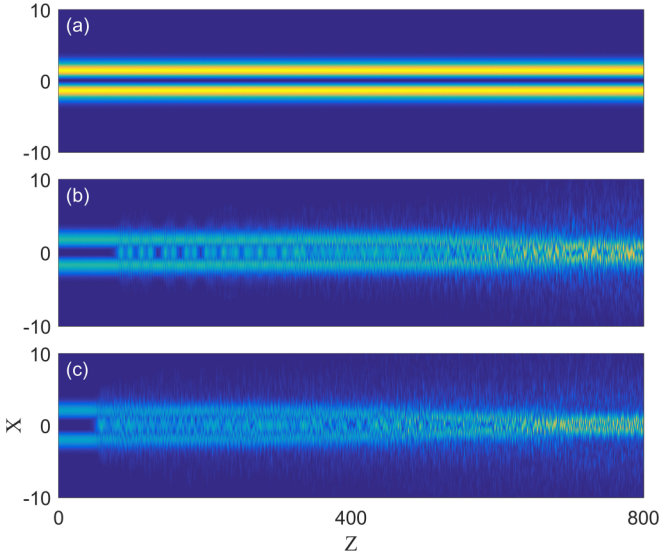
*zll_42@126.com
†linji@zjnu.edu.cn

054214-1

FIG. 1. Propagation of LG beams in lead glass for $p = 0$ and different m. The cross section through the $X = 0$ plane is shown. The parameters are chosen as (a) $m = 2$, $P_{02} = 38$; (b) $m = 3$, $P_{03} = 51$; (c) $m = 4$, $P_{04} = 63$.

FIG. 2. Evolution of the beam width (a), and of the correlation coefficient (b) of beams from Fig. 1.

nonlinear Schrödinger equation (NNLSE) [23,28,29]:

$$i\frac{\partial \psi}{\partial Z} + \frac{1}{2}\left(\frac{\partial^2}{\partial X^2} + \frac{\partial^2}{\partial Y^2}\right)\psi + G\psi = 0, \quad (1)$$

$$\left(\frac{\partial^2}{\partial X^2} + \frac{\partial^2}{\partial Y^2}\right)G = -|\psi|^2, \quad (2)$$

where $X = x/a_0$ and $Y = y/a_0$ are the transverse coordinates (i.e., scaled by the input beam width a_0), and $Z = z/ka_0^2$ is the longitudinal coordinate. Further, $\psi = (\alpha\beta\kappa^2 a_0^4/n_0\kappa)^{1/2}\Phi$ and $G = \kappa^2 a_0^2 \Delta n/n_0$ are dimensionless quantities of the complex field amplitude Φ, with $k = 2\pi n_0/\lambda$ being the wavenumber in media, and n_0 and Δn being the linear and nonlinear refractive index, respectively. Then, α, β, and κ represent the absorption, thermo-optical, and thermal conductivity coefficients of a lead glass sample, respectively [28,29].

Here, we choose an LG beam [30] as the initial condition in our numerical simulations,

$$\psi(r, \varphi, Z)|_{Z=0} = \sqrt{\frac{Pp!}{\pi(m+p)!}}\left[\frac{r}{a_0}\right]^m L_p^m\left[\frac{r^2}{a_0^2}\right]$$
$$\times \exp\left[-\frac{r^2}{2a_0^2} + im\varphi\right], \quad (3)$$

where $P = \iint |\psi|^2 dXdY$ is the beam power and $r = (X^2 + Y^2)^{1/2}$ is the radial distance. $L_p^m[\cdots]$ are the generalized Laguerre polynomials, with m and p being the azimuthal and radial mode numbers, respectively. $\varphi = \arctan(Y/X)$ is the azimuthal angle. According to the definition of the second-order moment [18,19], the statistical width of the beam is
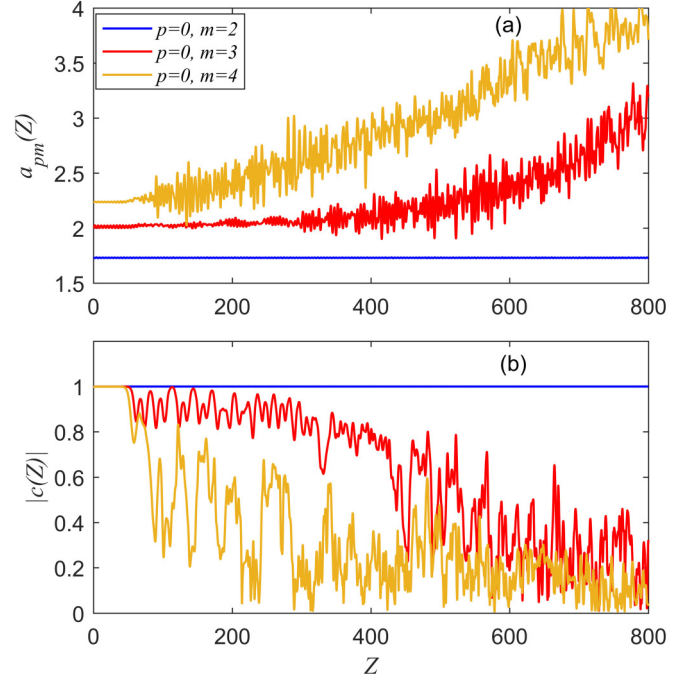
obtained by

$$a_{pm} = \sqrt{\frac{2\int_{-\infty}^{+\infty}\int_{-\infty}^{+\infty} X^2|\psi|^2 dXdY}{\int_{-\infty}^{+\infty}\int_{-\infty}^{+\infty} |\psi|^2 dXdY}}. \quad (4)$$

III. UNBOUNDED STATES AND CHAOTICONS

We investigate numerically the propagation of LG beams in lead glass by employing the standard split-step Fourier method. For convenience and without loss of generality, we set $a_0 = 1$ in all numerical simulations. In addition, the windows of the system in the X and Y directions both range from $-L/2$ to $L/2$, with $L = 100$ the sample width.

A. Unbounded states when $p = 0$

We start the discussion with the simplest case of $p = 0$, displayed in Fig. 1. Note that the low-order vortex modes $m = 0, 1, 2$ can form stable vortex solitons in lead glass, as confirmed in Refs. [22–24] and, as an example, we demonstrate the propagation of a stable vortex soliton with $m = 2$ in Fig. 1(a). However, the propagation of vortices with $m \geqslant 3$ in actual nonlocal nonlinear media is completely unstable. When selecting proper initial powers, the beams in Figs. 1(b) and 1(c) both propagate stably over a considerable distance, then break up and evolve into a set of single-hump profiles while emitting remnants of their energy. The radiation waves spread to infinity, resulting in an increasing beam width, as seen in Fig. 2(a). Obviously, such an unstable beam is in fact an unbounded state.

The proper input power, which makes the beam (ψ_{pm}) propagate stably initially (meaning that the beam diffraction
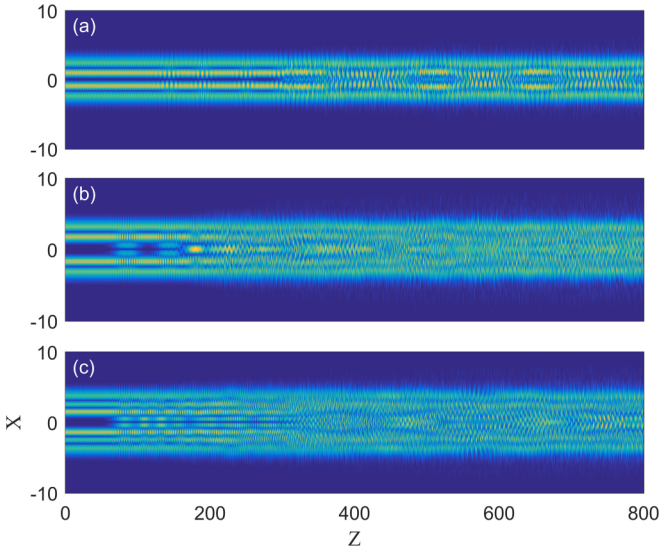
FIG. 3. Propagation of LG beams in lead glass for $p > 0$. The setup is as in Fig. 1. The parameters are chosen as $P = P_{pm}$, (a) $p = 1$, $m = 2$, $P_{12} = 64$; (b) $p = 1$, $m = 5$, $P_{15} = 101$; (c) $p = 2$, $m = 5$, $P_{25} = 127$.
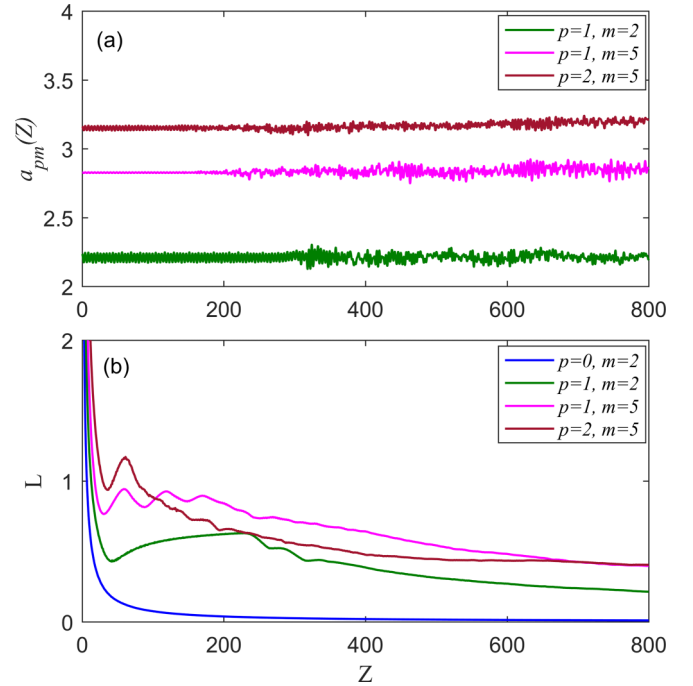

FIG. 4. Evolution of (a) beam width, and (b) maximal Lyapunov exponents of beams in Figs. 1 and 3. The parameters are chosen as those in Fig. 1 (blue lines) and Fig. 3 (green, pink, and brown lines).

is balanced by the nonlinearity) in Fig. 1, can be regarded as the critical power P_{pm}. However, when the beam expands or contracts initially (for example, as shown in Figs. 7(a1) and 7(b1), respectively), resulting from the beam diffraction being weaker or stronger than the nonlinearity, that means that the input power is smaller or larger than the critical power.

In addition, the comparison of Figs. 1(a)–1(c) shows that the instability of the optical beam increases with m, and the propagation distance before the breakup takes place becomes shorter and shorter. In fact, one can employ the cross-correlation function for more clearly observing the significant changes in the waveform,

$$c(Z) = \frac{1}{P} \int_{-\infty}^{\infty} \int_{-\infty}^{\infty} \psi(X, Y, 0)\psi^*(X, Y, Z)dXdY, \quad (5)$$

where the superscript * denotes the complex conjugate. The value of $|c|$ starts at 1, and remains constant for the soliton case ($m = 2$), whereas for $m = 3$ and 4, $|c|$ decreases with the increase of Z. Assuming $|c| = 0.95$ as the critical point where the waveform deforms significantly, the breakup positions of the waveform along the Z axis can be easily estimated from Fig. 2(b), which clearly agree with those seen in Fig. 1.

B. Vortex chaoticons when $p \geqslant 1$

When $p \geqslant 1$, Fig. 3 shows that the propagation of optical beams is still unstable and the beam profiles break up too. However, the intensity is localized well with very little scattering, which results in the beam width remaining statistically unchanged, while slightly oscillating irregularly. This is clearly seen in Fig. 4(a).

The positive Lyapunov exponent is a signature of chaos; hence we determine the maximal Lyapunov exponents for the evolution of unstable stationary solutions of vortex beams in lead glass. The maximal Lyapunov exponent can be

numerically obtained as [25,26]

$$L = \lim_{\varepsilon \to 0} \lim_{Z \to \infty} \frac{1}{Z} \ln \frac{d(\psi_1, \psi_2; Z)}{d(\psi_1, \psi_2; 0)}, \quad (6)$$

$$d(\psi_1, \psi_2; Z) = \left[\int_{-\infty}^{\infty} \int_{-\infty}^{\infty} |\psi_1(X, Y, Z) \right.$$

$$\left. - \psi_2(X, Y, Z)|^2 dXdY \right]^{1/2}, \quad (7)$$

where $d(\psi_1, \psi_2; Z)$ is the distance between two functions $\psi_1(X, Y; Z)$ and $\psi_2(X, Y; Z)$ in the Hilbert space (the L^2 norm in the Hilbert space); the initial values are $\psi_1(X, Y; 0) = \psi(X, Y; 0)$ and $\psi_2(X, Y; 0) = \psi(X, Y; 0) + \delta(X, Y)$, where $\delta(X, Y)$ is a random perturbation function (as small as the machine precision allows, e.g., of the order of 10^{-7}). Using the same procedure as in Refs. [25,26], the curves of the maximal Lyapunov exponents are obtained, as shown in Fig. 4(b). One can see that the curve of the maximal Lyapunov exponent of the vortex soliton ($p = 0$, $m = 2$) approaches 0. However, for unstable beams, they approach positive values, which is sufficient to indicate the chaotic behavior along the Z direction.

Figure 5 shows concretely the intensity variation of an unbounded state and a chaoticon in the transverse cross section during propagation. One can see that both of these beams can quasistably propagate for a certain distance before breaking up, the difference being that most of the intensity spreads out and leaves a single peak in Fig. 5(a4), whereas in Fig. 5(b4) the intensity remains localized well.

The spiral flow of the electromagnetic energy of vortex beams results in the nonzero OAM, which is an important concept deserving special attention. The OAM can be obtained by
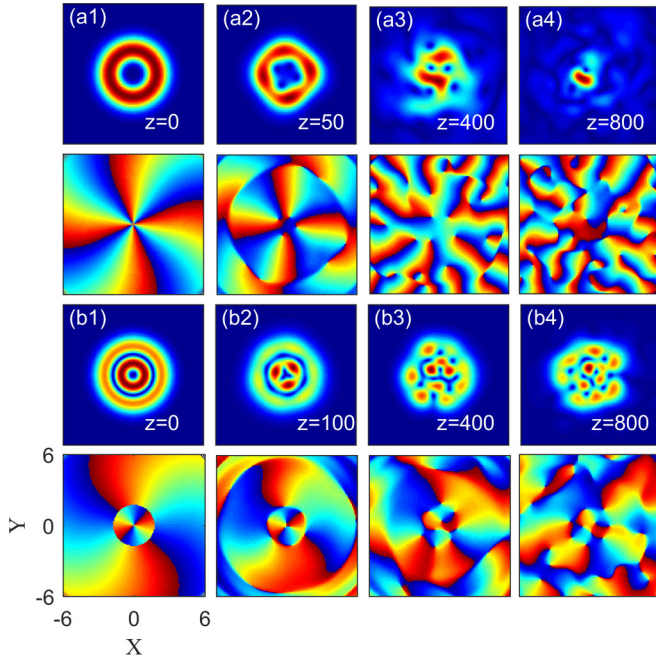
FIG. 5. Comparison of an unbounded state beam and chaoticon in the transverse cross section during propagation. The parameters of (a1–a4) and (b1–b4) are chosen as those in Figs. 1(b) and 3(a), respectively. The second and fourth rows depict the corresponding phase evolution.
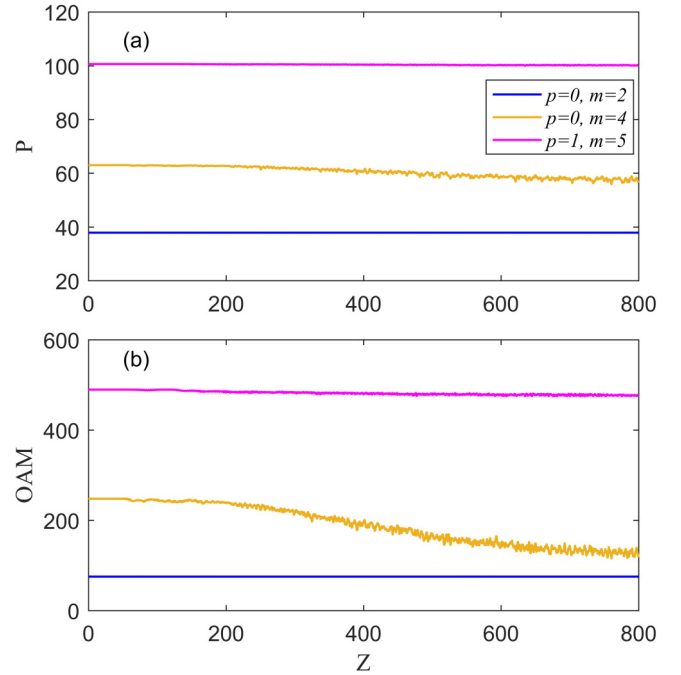

FIG. 6. Evolution of power (a) and OAM (b), for the soliton (blue line), unbounded state beam (yellow line), and chaoticon (pink line). The parameters of blue, yellow, and pink lines are all chosen as those in Figs. 1(a), 1(b), and 2(b), respectively.

Eq. (8) [18,19]:

$$M = \mathrm{Im} \int_{-\infty}^{\infty} \int_{-\infty}^{\infty} \psi^* \left(X \frac{\partial \psi}{\partial Y} - Y \frac{\partial \psi}{\partial X} \right) dX dY. \qquad (8)$$

Recalling that the intensity of the unstable beams displays more or less scattering, investigating the retained power and OAM of the intensity distribution only in the central region ($X, Y \in [-6, 6]$) has the actual application value. The blue lines in Fig. 6 show that the soliton can maintain its power and OAM very well during propagation. It is surprising that the power and OAM of the chaoticon remain almost unchanged (pink line), while those of the unbounded state beam decay fast in the central region (yellow line), due to intense scattering.

IV. OTHER PROPAGATION PROPERTIES OF VORTEX CHAOTICONS

When the input power is not equal to the critical power, the vortex beams ($m \leqslant 2$) will evolve into breathers and present a periodically oscillating width during propagation [17,22]. For the chaoticons, such as exemplified in Fig. 3(c), when the input power is equal to $1.3P_{25}$ and $0.7P_{25}$, Fig. 7(a1)–7(c1) show that the vortex beams will evolve into breathers in a short propagation distance. However, after a long distance, the beams will break up and are localized well too, without any energy lost by radiation during the evolution, and both widths maintain well their values, as seen in Figs. 7(a2)–(c2). Different statistical beam widths corresponding to different input powers are another feature of chaos, which is sensitive to the initial value.

Figure 8(a) demonstrates the particlelike interaction phenomenon between two vortex solitons, which is another typical property of an optical soliton. Obviously, similar interaction in the quasielastic collision of two identical chaoticons also exists, as shown in Figs. 8(b) and 8(c). However, after the long propagation distance, both the interacting solitons and chaoticons will merge into a single local beam with
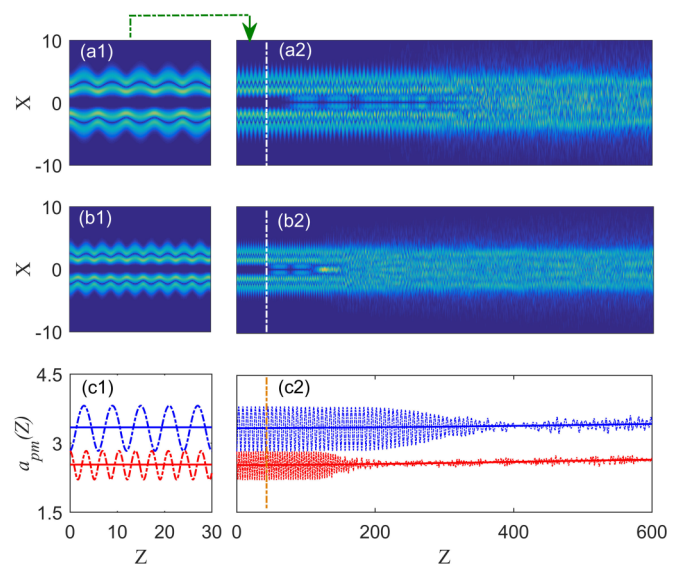

FIG. 7. Evolution of vortex chaoticons in lead glass with $P = 1.3P_{25}$ (a) and $P = 0.7P_{25}$ (b). Evolutions of beam widths are depicted as dashed blue and red lines in (c), and solid lines are the corresponding mean values.
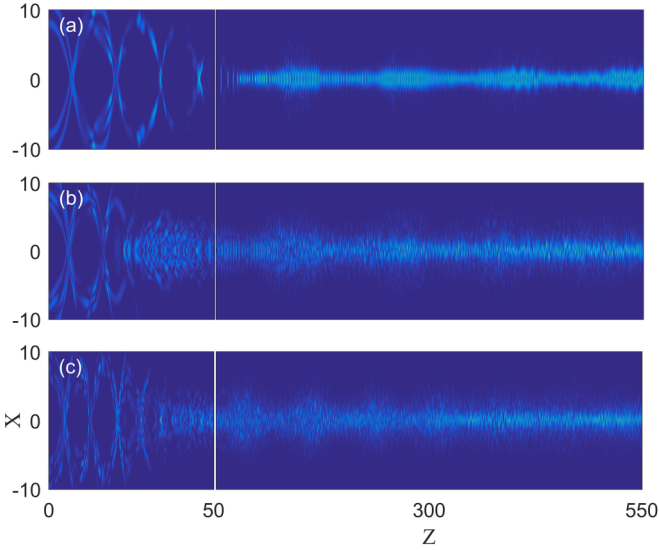
FIG. 8. Incoherent interaction in quasielastic collisions between two initially parallel identical beams. The parameters of beams in (a)–(c) are all chosen as those in Figs. 1(a), 2(b), and 2(c), respectively.
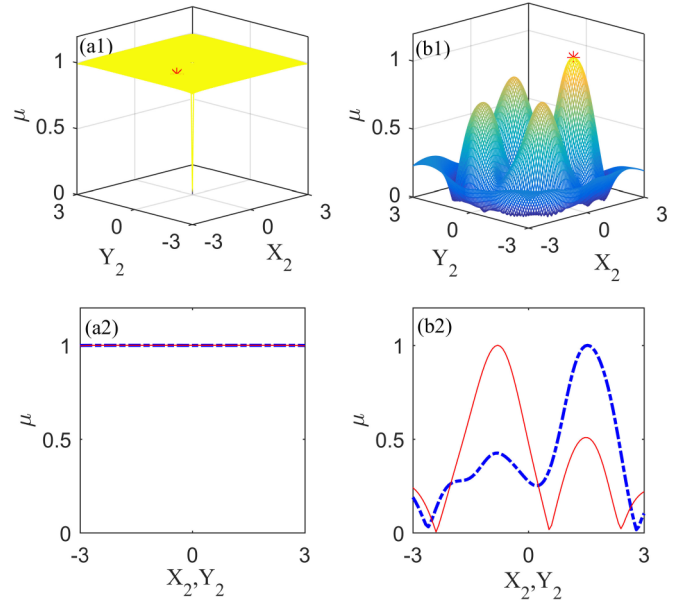

FIG. 9. Spatial cross correlation of the red asterisk point with other points in space for the soliton (a1) and chaoticon (b1), whose parameters are chosen as those in Figs. 1(a) and 3(b), respectively. (a2), (b2) The spatial cross-correlation function of (a1), (b1) in $X_2 = 1$ (red lines) and $Y_2 = 1$ (blue lines) directions.

periodically oscillating width and, rarely, scattering. It should be pointed out that the initial chaoticons are $\psi(X, Y, Z_0)$ for $Z_0 \geqslant 200$, in order to ensure that the inputs are completely irregular states.

Actually, with respect to time and space, there are two kinds of chaotic states for a partial differential equation system: the temporal chaos with spatial coherence and the spatiotemporal chaos with spatial decoherence [25–27]. Hence, for making the type of our chaotic solutions clear, we calculate the spatial cross-correlation function of two long-enough wave-amplitude series at locations (X_1, Y_1) and (X_2, Y_2):

$$\mu[(X_1, Y_1), (X_2, Y_2)]$$
$$= \lim_{Z \to \infty} \frac{\int_0^{Z_0} \psi(X_1, Y_1, Z)\psi^*(x_2, Y_2, Z)dZ}{\sqrt{\int_0^{Z_0} |\psi(X_1, Y_1, Z)|^2 dZ \int_0^{Z_0} |\psi(X_2, Y_2, Z)|^2 dZ}}. \tag{9}$$

Without loss of generality, here we arbitrarily select one point $(X_1 = 1, Y_2 = 1)$, which is marked by a red asterisk, and then calculate the spatial cross-correlation function of such a point with all other points in space, as shown in Fig. 9. One can see that $|\mu|$ equals 1 for solitons, and decreases rapidly

around the red asterisk point for chaoticons. The quick drop of correlation signifies the spatial decoherence.

V. CONCLUSION

In summary, this paper demonstrates the existence of vortex chaoticons, which are formed by LG beams in cases when $p \geqslant 1$, in lead glass. The vortex chaoticons exhibit both chaotic and solitonlike properties. The chaotic behavior is marked by positive maximal Lyapunov exponents and spatial decoherence. The solitonlike properties include the invariant statistical width and the quasielastic collision during interaction of the beams. In addition, we find that the power and OAM of an unbounded state beam both display strong decay, whereas those of chaoticons maintain their values very well.

[1] R. Barboza, U. Bortolozzo, G. Assanto, E. Vidal-Henriquez, M. G. Clerc, and S. Residori, Harnessing Optical Vortex Lattices in Nematic Liquid Crystals, Phys. Rev. Lett. **111**, 093902 (2013).

[2] R. Barboza, U. Bortolozzo, G. Assanto, E. Vidal-Henriquez, M. G. Clerc, and S. Residori, Vortex Induction via Anisotropy Stabilized Light-Matter Interaction, Phys. Rev. Lett. **109**, 143901 (2012).

[3] M. Piccardo, M. D. Oliveira, A. Toma, V. Aglieri, A. Forbes, and A. Ambrosio, Vortex laser arrays with topological charge control and self-healing of defects, Nat. Photonics **22**, 359 (2022).

[4] D. Liu, C. Zhou, P. Lu, J. Xu, Z. Yue, and S. Teng, Generation of vector beams with different polarization singularities based on metasurfaces, New J. Phys. **24**, 043022 (2022).

[5] S. Bernet, A. Jesacher, S. Furhapter, C. Maurer, and M. Ritsch-Marte, Quantitative imaging of complex samples by spiral phase contrast microscopy, Opt. Express **14**, 3792 (2006).

[6] M. Chen, M. Mazilu, Y. Arita, E. M. Wright, and K. Dholakia, Dynamics of microparticles trapped in a perfect vortex beam, Opt. Lett. **38**, 4919 (2013).

[7] M. Padgett and R. Bowman, Tweezers with a twist, Nat. Photonics **5**, 343 (2011).

[8] M. Gecevičius, R. Drevinskas, M. Beresna, and P. Kazansky, Single beam optical vortex tweezers with tunable orbital angular momentum, Appl. Phys. Lett. **104**, 231110 (2014).

[9] V. Pravin and L. Rusch, Perfect vortex beam: Fourier transformation of a Bessel beam, Opt. Lett. **40**, 597 (2015).

[10] F. Yue, D. Wen, J. Xin, B. Gerardot, J. Li, and X. Chen, Vector vortex beam generation with a single plasmonic metasurface, ACS Photonics **3**, 1558 (2016).

[11] H. Xu, H. Liu, X. Ling, Y. Sun, and F. Yuan, Broadband vortex beam generation using multimode Pancharatnam–Berry metasurface, IEEE Trans. Antennas Propag. **65**, 7378 (2017).

[12] Y. Hira and Y. Monnai, Sub-terahertz vortex beam generation using a spiral metal reflector, Opt. Express **29**, 24118 (2021).

[13] L. Zeng, B. A. Malomed, D. Mihalache, Y. Cai, X. Lu, Q. Zhu, and J. Li, Bubbles and W-shaped solitons in Kerr media with fractional diffraction, Nonlinear Dyn. **104**, 4253 (2021).

[14] L. Zeng and J. Zeng, One-dimensional gap solitons in quantic and cubic-quintic fractional nonlinear Schrödinger equations with a periodically modulated linear potential, Nonlinear Dyn. **98**, 985 (2019).

[15] O. Bang, W. Krolikowski, J. Wyller, and J. J. Rasmussen, Collapse arrest and soliton stabilization in nonlocal nonlinear medium, Phys. Rev. E **66**, 046619 (2002).

[16] D. Briedis, D. E. Petersen, D. Edmundson, W. Krolikowski, and O. Bang, Ring vortex solitons in nonlocal nonlinear medium, Opt. Express **13**, 435 (2005).

[17] D. Deng and Q. Guo, Propagation of Laguerre-Gaussian beams in nonlocal nonlinear medium, J. Opt. A: Pure Appl. Opt. **10**, 035101 (2008).

[18] Q. Wang and Z. Deng, Controllable propagation path of imaginary value off-axis vortex soliton in nonlocal nonlinear media, Nonlinear Dyn. **100**, 1589 (2020).

[19] G. Liang and Q. Wang, Rotation controlling of spiraling elliptic beams in inhomogeneous nonlocal media, New J. Phys. **23**, 103036 (2021).

[20] L. Song, Z. Yang, S. Zhang, and X. Li, Spiraling anomalous vortex beam arrays in strongly nonlocal nonlinear media, Phys. Rev. A **99**, 063817 (2019).

[21] T. P. Horikis and D. J. Frantzeskakis, Ring dark and antidark solitons in nonlocal media, Opt. Lett. **41**, 583 (2016).

[22] U. A. Laudyn, M. Kwasny, M. Karpierz, and G. Assanto, Vortex nematicons in planar cells, Opt. Express **28**, 8282 (2020).

[23] H. Zhang, M. Chen, L. Yang, B. Tian, C. Chen, Q. Guo, Q. Shou, and W. Hu, Higher-charge vortex solitons and vector vortex solitons in strongly nonlocal medium, Opt. Lett. **44**, 3098 (2019).

[24] Y. V. Izdebskaya, V. G. Shvedov, P. S. Jung, and W. Krolikowski, Stable vortex soliton in nonlocal medium with orientational nonlinearity, Opt. Lett. **43**, 66 (2018).

[25] L. Zhong, Y. Li, Y. Chen, W. Hong, W. Hu, and Q. Guo, Chaoticons described by nonlocal nonlinear Schrödinger equation, Sci. Rep. **7**, 41438 (2017).

[26] L. Zhong, Q. Guo, W. Hu, W. Hong, and W. Xie, Chaotic self-trapped optical beams in strongly nonlocal nonlinear media, Phys. Rev. A **99**, 043816 (2019).

[27] N. Verschueren, U. Bortolozzo, M. G. Clerc, and S. Residori, Spatiotemporal Chaotic Localized State in Liquid Crystal Light Valve Experiments with Optical Feedback, Phys. Rev. Lett. **110**, 104101 (2013).

[28] H. Zhang, T. Zhou, Q. Shou, and Q. Guo, Optical elliptic breathers in isotropic nonlocal nonlinear media, Opt. Express **30**, 9636 (2022).

[29] S. A. Louis, T. R. Marchant, and N. F. Smyth, 2-D solitary waves in thermal media with nonsymmetric boundary conditions, Stud. Appl. Math. **142**, 586 (2019).

[30] B. A. Malomed, Vortex solitons: Old results and new perspectives, Physica D (Amsterdam) **399**, 108 (2019).

Correction: The previously published Figure 4 contained an incorrect axis label and has been replaced. A project number in the Acknowledgment section was incorrect and has been fixed.